Complete polarization control for a nanofiber waveguide using the scattering properties

Maxime Joos, Alberto Bramati, Quentin Glorieux

Research Article | Vol. 27, No. 13 | 24 Jun 2019 | OPTICS EXPRESS 18818
Optics EXPRESS

Complete polarization control for a nanofiber waveguide using the scattering properties

MAXIME JOOS, ALBERTO BRAMATI, AND QUENTIN GLORIEUX*

Laboratoire Kastler Brossel, Sorbonne Université, CNRS, ENS-PSL Research University, Collège de France, Paris, France
*quentin.glorieux@lkb.upmc.fr

Abstract: We report on a protocol to achieve full control of the polarization in a nanofiber. The protocol relies on monitoring the light scattered out from a nanofiber by means of two optical systems with 45° camera angle difference. We study the disturbance of the nanofiber refractive index on the radiation of embedded scatterers, and we propose an explanation for the observed reduced scattering contrast of the nanofiber. Thanks to this approach, we demonstrate an accuracy of the polarization control larger than 95%.

1. Introduction

Optical nanofibers have drawn increasing attention in the last decade as a scalable light-matter interface. They naturally provide large light-matter coupling strength due to the tight confinement of the guided light and enable easy interfacing with emitters through their evanescent fields [1, 2]. Recently, it was realized that optical nanofibers are also privileged interfaces to study and exploit light-matter chiral processes [3–6]. These developments require a precise control of the polarization of the light guided in the nanofiber. Primarily for the trapping geometry [7, 8] and secondly for the probe beams in order to address specific radiative transitions.

Optical nanofibers are produced by locally heating and pulling commercial single-mode fibers [9]. The guided light propagating towards or from the nanofiber is subject to birefringence [10] of the optical fibers. Birefringence can be specific to the fiber, as for example the residual ellipticity of the core or internal stress. Birefringence can else be due to the manipulation of the fiber (bending, twisting) or to its environment (temperature, pressure). The polarization is therefore not maintained in general when light propagates through a fiber. This issue makes it difficult to control the polarization in nanofibers and has been a challenge for the nanofiber community for years. Until now, the control has been limited to aligning the polarization quasi-linearly along two fixed orthogonal axis [11, 12].

In this work, we show that the full control of the polarization can be achieved so that it is possible to deterministically set an arbitrary polarization in a nanofiber with good accuracy. This new capability holds great promises in nanofiber experiments as it opens the way for exotic dipole trapping geometries [13, 14], magneto-optical trapping through the guided fields, new interactions with nanoparticules [15] and atomic ensembles [16, 17].

Controlling the polarization in a nanofiber enables reciprocally to read an unknown polarization of the fundamental mode in a nanofiber [18]. Recently, this capability was used to analyze the emission properties of gold nanorods deposited at the surface of an optical nanofiber [15].

The paper is organized as follow. First, we formally introduce the strategy for compensating the birefringence in an optical fiber in order to control the polarization of the fundamental mode in the nanofiber region. In section 3, we detail the ideal procedure to compensate the birefringence of an optical system, which includes the optical fiber, using a variable wave retarder (Berek compensator). In section 4, we address a limitation of the ideal compensation procedure, namely the effect of the dielectric nanofiber on the embedded radiating dipoles. We employ Mie theory and numerical simulations. In section 5, we propose an update of the ideal procedure of section

#362732 https://doi.org/10.1364/OE.27.018818
Journal © 2019 Received 25 Mar 2019; revised 15 May 2019; accepted 17 May 2019; published 20 Jun 2019

Optics EXPRESS

3 to take into account this effect. Finally, we present in section 6 our test procedure and show compensation data with an accuracy better than 95%.

2. Matrix formulation of the problem

We consider the typical nanofiber setup presented in Fig. 1, where the light is coupled into a single mode fiber and guided trough the nanofiber. Light also passes through several passive optical elements like mirrors or lenses, but these elements are not represented in Fig. 1, for clarity. The free-space polarization before the setup is controllable by usual means (for example using a combination of wave plates) and it is represented by the Stokes vector $\mathbf{S}_{in}$. The polarization of the fundamental mode in the nanofiber is represented by the Stokes vector $\mathbf{S}_{out}$. The general problem we discuss in this paper is: how to achieve a specific polarization of the guided light in the nanofiber region?

The strategy consists in transferring the controllable polarization state $\mathbf{S}_{in}$ in the nanofiber region. This requires to compensate the birefringence introduced by the fiber system, represented by the Müller matrix $\mathcal{M}_f$. The birefringence compensation is achieved by placing a variable wave retarder (more specifically a Berek compensator) –represented by the Müller matrix $\mathcal{M}_B$– before the optical system.

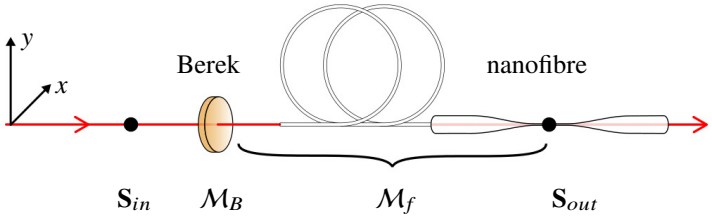

Fig. 1. Nanofiber setup. Typical nanofiber setup to set the polarization of the guided light in the nanofiber region despite an arbitrary birefringence of the fiber. The input polarization state is denoted $\mathbf{S}_{in}$. Light propagates through a Berek compensator (represented by the Müller matrix $\mathcal{M}_B$), a fiber system (represented by $\mathcal{M}_f$) and ends up with polarization state $\mathbf{S}_{out}$ in the nanofiber region.

If the phase shift introduced by the variable wave retarder ($\mathcal{M}_B$) is opposite to the phase shift introduced by the fiber system ($\mathcal{M}_f$), the net birefringence of the overall system is zero. In this compensated case, the polarization in the nanofiber ($\mathbf{S}_{out}$) is a replica of the input polarization ($\mathbf{S}_{in}$). Therefore the polarization control over the input state has been extended to the nanofiber light.

The Berek compensator is a simple realization of a variable wave retarder. It consists of an uni-axial crystal plate (typically calcite or magnesium fluoride) cut in such a way that its extraordinary axis is perpendicular to the optical faces. Tilting the plate enables to introduce a variable phase shift between the two polarization components while rotating the plate orient the optical axes. In our experiment, we use a mechanical mount that enables to adjust each degree of freedom (retardance and optical axes orientation) independently (see for example the commercial model 5540M from Newport). At our working wavelength ($\lambda = 638$ nm), the phase shift can be adjusted in the range $0 - 2\pi$.

In the following, we first recall the matrix formalism which describes the transformation of polarization by the system (composed of the Berek and the fiber system) in the general case. We then consider formally the special case of interest where birefringence is compensated. Within the Stokes-Müller formalism, we can write:

$$\mathbf{S}_{out} = \mathcal{M}_f \mathcal{M}_B \mathbf{S}_{in}. \tag{1}$$

Optics EXPRESS

The matrix $\mathcal{M}_f$ describes an arbitrary bent optical fiber which induces birefringence [19] and optical rotation [20]. Birefringence will typically affect the ellipticity of the polarization while the optical rotation will rotates the polarization axes. This is represented by the combination of a linear retarder and a rotator [20–22]:

$$\mathcal{M}_f = \mathcal{S}(\theta)\mathcal{G}(\delta, \phi) \tag{2}$$

where $\mathcal{S}(\theta)$ is a rotation matrix:

$$\mathcal{S}(\theta) = \begin{pmatrix} 1 & 0 & 0 & 0 \\ 0 & \cos(2\theta) & -\sin(2\theta) & 0 \\ 0 & \sin(2\theta) & \cos(2\theta) & 0 \\ 0 & 0 & 0 & 1 \end{pmatrix}, \tag{3}$$

and $\mathcal{G}(\delta, \phi)$ describes a wave retarder with retardance δ and fast axis at angle ϕ, and

$$\mathcal{G}(\delta, \phi) = \mathcal{S}(\phi) \begin{pmatrix} 1 & 0 & 0 & 0 \\ 0 & 1 & 0 & 0 \\ 0 & 0 & \cos(\delta) & -\sin(\delta) \\ 0 & 0 & \sin(\delta) & \cos(\delta) \end{pmatrix} \mathcal{S}(-\phi). \tag{4}$$

Hence the effect of the bent fiber on the polarization is determined by three parameters: the phase shift δ and the fast axis orientation ϕ of the equivalent retarder, and the rotation θ of the equivalent rotator.

The goal of the compensation procedure is to adjust the two degrees of freedom of the Berek compensator to induce a birefringence opposite to the equivalent retarder represented by $\mathcal{G}(\delta, \phi)$, i.e if $\mathcal{M}_B = \mathcal{G}(\delta, \phi)^{-1}$. By doing so, the overall optical system of Eq. (1) reduces simply to an optical rotator:

$$\mathcal{M}_f \mathcal{M}_B = \mathcal{M}_f \mathcal{G}(\delta, \phi)^{-1} = \mathcal{S}(\theta). \tag{5}$$

In the case of birefringence compensation, the polarization state in the nanofiber $\mathbf{S}_{out}$ is hence a rotated replica of the input polarization $\mathbf{S}_{in}$. This rotation by an angle θ can be easily measured and taken into account. We therefore have a situation where we can deterministically prepare a polarization at the input of the system and have this polarization reproduced in the nanofiber. This situation corresponds to having the complete control of the polarization state in the nanofiber region. In the following section, we introduce the figure of merit that enables to adjust properly the Berek compensator.

3. Berek compensation: ideal case

The Berek compensation relies on studying the light scattered in the nanofiber region. The microscopic origin of this scattering is not a well documented topic. Surface imperfections and localized random inhomogeneities in the bulk were suggested to be at the origin of the scattering [11]. The presence of dopants and impurities cannot be excluded neither. For now, we assume that scattering originates from point-like sources and conserves the polarization of the incident guided light.

Therefore, we can have access to some crucial information on the guided polarization by looking at the scattered light. We further assume that the nanofiber refractive index does not alter the radiation pattern of the scatterers. For example, if the guided light is vertically polarized

Optics EXPRESS

in the nanofiber, as illustrated in Fig. 2(b), we assume the azimuthal radiation pattern to be dipole-like (following a pattern in $\cos^2$).

Consider now the fiber setup of Fig. 2(a) where two cameras are used to collect the scattered light from the nanofiber. One camera is positioned horizontally and faces the x axis. The second camera is positioned 45° above the first camera. Both cameras look at the same region of the nanofiber and have optical axes orthogonal to the nanofiber axis (z). The cameras are further equipped with linear polarizers aligned perpendicularly with respect to the nanofiber z-axis and to the optical axis of the camera. In this position, the polarizers filter out the longitudinal (along z) component and transmit only the transverse component of the scattered light. This filtering stage considerably simplifies the analysis [11].

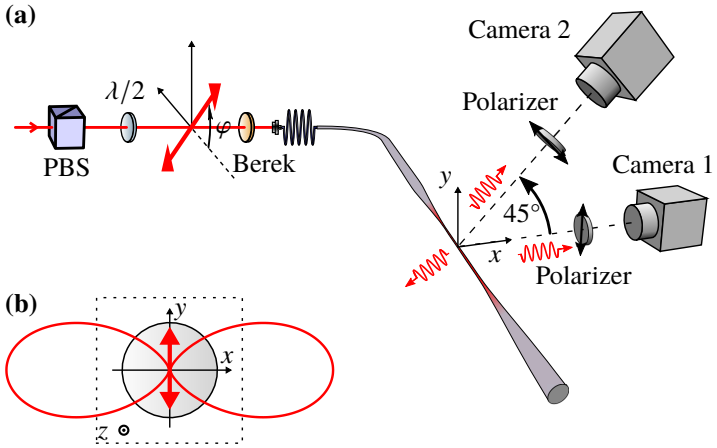

Fig. 2. Berek compensation setup. (a) Experimental setup. Linearly polarized light is prepared with a polarized beam splitter PBS, followed by a half-wave plate and sent in the optical system including the Berek compensator and the fiber. A small fraction of the guided light in the nanofiber is scattered out and collected by two optical systems with different angles. The cameras are equipped with polarizers filtering out the longitudinal (along z) component of the scattered light. Because scattering is supposed to be polarization maintaining, the study of the scattered light enables to infer the guided polarization. A position of the Berek compensator can be found to have the output polarization state $\mathbf{S}_{out}$ being a replica of the input polarization $\mathbf{S}_{in}$. (b) Transverse representation of the nanofiber showing the scattering pattern of the guided light in the case of vertical polarization of the fundamental mode (neglecting the longitudinal component of the field). We assume the radiation pattern of a dipole in vacuum.

The exact radiation pattern of a dipole in a nanofiber (with a refractive index larger than 1) can be simulated numerically and differs slightly from the $\cos^2$ dependence expected for a linear dipole in vacuum (see section 4). In first approximation, we assume a linear dipole radiation and therefore a radiation pattern with a $\cos^2$ dependence, as illustrated in Fig. 2(b) (departure from this ideal case is considered in section 4). This approximation simplifies greatly the formalism because the radiation pattern has the same angle dependence as the projection of the dipole on the vertical axis.

Hence, the signal collected by the horizontal camera, called I_1, is proportional to the intensity of guided light polarized vertically. The signal collected by the second camera at 45°, called I_2, is proportional to the intensity of light polarized at 135°. As an example, we describe the radiation signal detected by camera 1 (at horizontal) for a few specific guided polarizations in the nanofiber. For vertical (horizontal) quasi-linear polarization of the fundamental mode, the signal collected by camera 1 is maximal (minimal, zero in the ideal case). For quasi-linearly polarized

Optics EXPRESS

light at 45° as well as for circular polarization, the signal collected by camera 1 is half of the maximum value. I_1 and I_2 are closely related to the normalized Stokes parameters S^1_{out} and S^2_{out} of the guided light. From the definition of the Stokes parameters, one gets:

$$\begin{aligned} S^1_{out} &= -\frac{I_1 - \overline{I_1}}{\overline{I_1}} \\ S^2_{out} &= -\frac{I_2 - \overline{I_2}}{\overline{I_2}} \end{aligned} \tag{6}$$

where $\overline{I_1}$ and $\overline{I_2}$ are half of the maximum signals corresponding to vertically polarized light and linearly polarized light at 135° respectively. Linear polarization of the guided light is characterized by $(S^1_{out})^2 + (S^2_{out})^2 = 1$. We therefore have a measurable criteria (based on the scattered light by the nanofiber) to identify linear polarization of the guided light in the nanofiber.

Within the ideal frame of dipole like radiation, we propose the following procedure to adjust the Berek compensator:

1. First, place the Berek compensator in a neutral position, or equivalently remove the Berek. Then, search for the linear polarization at the input that gives rise to linear polarization in the nanofiber region. We denote this input polarization angle φ_0. In practice, linear polarization at angle φ is prepared using a horizontal polarizer followed by a motorized half-wave plate (see Fig. 2(a)). In other words, this step corresponds to aligning the input polarization with respect to the optical axes of the effective wave retarder of the fiber system represented by $\mathcal{G}(\delta, \phi)$, i.e. $\varphi_0 = \phi$.

2. Second, align the optical axis of the Berek with respect to $\varphi_0 = \phi$. From this position, rotate the input linear polarization by 45°. This input polarization will, in general, give rise to an elliptical polarization in the nanofiber because the fiber system acts as a variable-wave retarder (plus optical rotation).

3. Finally, tilt the Berek plate, i.e. act on the variable phase shift, until a linear polarization in the nanofiber region is recovered. By doing so, a retardance $-\delta$ has been introduced, that is opposite to the retardance of the fiber system $\mathcal{M}_f$. The overall optical system has zero net birefringence.

An analog correction procedure has been proposed recently in [23]. Our procedure differs from [23] by the different pair of input states chosen as well as a different figure of merit to identify polarizations in the nanofiber region.

The deductive character of the Berek procedure relies, for the derivation of Eq. (6), on the assumption that scatterers in the nanofiber have dipole-like radiation patterns (see Fig. 2(b)). As we will show in the following, the nanofiber refractive index alters the radiation pattern of the embedded scatterers. This effect needs to be taken into account and requires to adapt the Berek procedure presented above.

4. Radiation pattern of dipoles in a nanofiber

In order to have a better understanding on how the scattered light by the nanofiber gives information on the polarization of the guided light, we investigate numerically the radiation of individual linear dipoles located in the bulk of a nanofiber.

To compute the dipole radiation patterns, we employ the diffraction theory of a plane wave by a dielectric cylinder, which we refer to as Mie theory [24, 25]. We present in the Fig. 3(a) the simulated far-field intensity radiation patterns of individual vertical dipoles in a nanofiber. We assumed a silica nanofiber (refractive index $n = 1.46$) with diameter of 300 nm surrounded by

Optics EXPRESS

air or vacuum (refractive index $n = 1.00$). The scattered light is assumed to have a wavelength in vacuum of 638 nm. We consider dipoles at different location in the nanofiber section. Only dipoles located exactly on the y axis do not radiate light in the vertical direction (i.e. along the dipole orientation). On contrary, dipoles not in the nanofiber center radiate along the dipole direction in strong contrast to the case of free space radiation.

We now simulate how the individual scatterers contribute to the average signal recorded by the camera (see Fig. 2(a)). A typical microscope image of a 300 nm nanofiber is presented in Fig. 3(b). We note that the scattering of light is not homogeneous over the length of the nanofiber which is consistent with the hypothesis of individual scatterers distributed randomly along the nanofiber. In order to extract from the nanofiber image a meaningful signal, we must integrate the image over a region of interest (ROI) that includes a large number of scatterers (see Fig. 3(b)). This portion of the nanofiber is typically a few hundred microns long.

We model the nanofiber portion as composed of a large number of adjacent cylindrical slices with thicknesses equal to the optical resolution of the optical system. If there is no more than one scatterer per such slice, i.e if all the scatterers of the nanofiber are optically resolved, the scatterers contribute independently to the integrated camera signal. In this case, we can simulate the integrated signal by summing the intensity radiation pattern of each individual scatterer, assuming that scatterers are randomly distributed in the transverse plane (xy) of the nanofiber.

In the case of scatterers that are not optically resolved, i.e if at least two scatterers are confined within such a slice of the nanofiber portion, these scatterers interfere on the image plane and contribute coherently to the detected signal. The spatially integrated camera signal would differ significantly from the previous case in a way that we will precise in the following.

Experimentally, to characterize the radiation scattered by a region of interest of the nanofiber, we define a visibility parameter:

$$V = \frac{I_{max} - I_{min}}{I_{max} + I_{min}}, \tag{7}$$

where I_{max} is the maximum camera signal which is obtained when the polarization is quasi-linear and orthogonal to the camera optical axis; I_{min} is the minimum camera signal obtained when the polarization is quasi-linear and oriented towards the camera. I_{max} and I_{min} are scattering intensities integrated over a region of interest as shown in Fig. 3(b). In the limit of a nanofiber diameter much smaller than the wavelength, the radiation pattern of embedded linear dipoles are following a $\cos^2$ dependence (similar to a dipole in vacuum) and a visibility of 1 is expected, expressing the fact that there is no scattering in the direction of the linear dipole axes.

Based on Mie theory, we present in Fig. 3(c) simulations of the average visibility of a portion of nanofiber as a function of the nanofiber diameter (expressed in unit of $\lambda = 638$ nm). We consider various possible distributions for the scatterers. Regarding the transverse distribution, we assume scatterers randomly and homegeneously distributed in the bulk of the nanofiber (solid lines of Fig. 3(c)) and scatterers randomly distributed at the surface of the nanofiber (dashed lines of Fig. 3(c)). Considering the longitudinal distribution, we assume different densities: 0.5, 4 and 20 scatterers per unit of optical resolution.

Finally, we compare our simulations with the measured visibilities observed in our experiment (LKB) and in the literature by Vetsch et al. [11] (Vetsch). We produced three nanofibers of diameters 260 nm, 300 nm and 327 nm starting from a commercial single-mode fiber (SM600 from Thorlabs, Cut-off wavelength 550 ± 50 nm, numerical aperture 0.12 ± 0.02, attenuation ≤ 15 dB/km) and using a standard heat-and-pull process [9]. Diameters are calibrated with less than 5 nm uncertainty using a scanning electron microscope. The measured visibilities are larger for thinner nanofibers which is a feature predicted by our simulations. At low scatterer density, the general trend of our simulations is that the visibility drops with the diameter of the nanofiber. For very small diameters ($2a/\lambda \ll 1$), the visibility tends to equal 1 meaning that the fiber does less alter the radiation of embedded scatterer. A larger density of scatterer per unit of optical

Optics EXPRESS

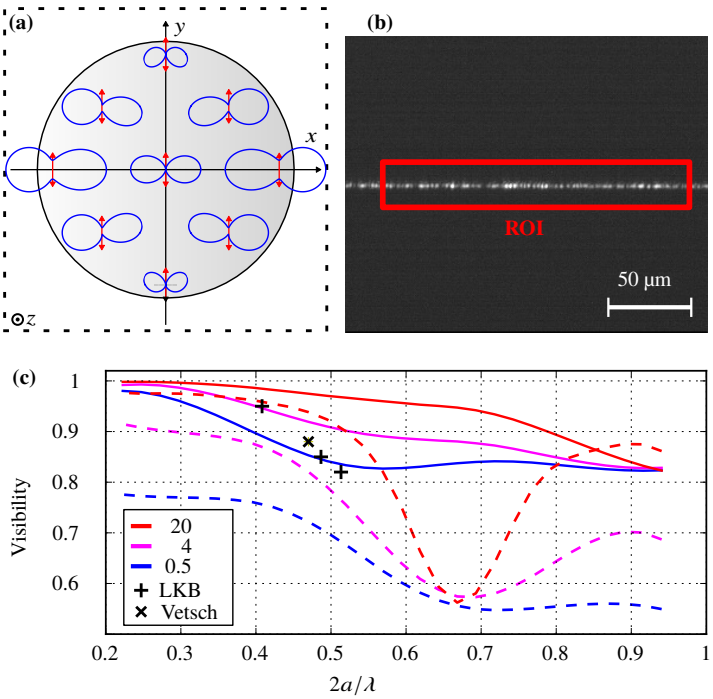

Fig. 3. Guided light scattering in a nanofiber. (a) Far-field radiation patterns of linear dipoles located in the bulk of a nanofiber computed according to Mie theory. The radiation significantly differs from the free-space case and depends on the position of the scatterer in the transverse plane of the nanofiber. (b) Typical microscope image of a nanofiber scattering its guided light as seen from one of the cameras. Scaterring intensity and visibility are obtained by integrating the camera signal over the entire region of interest (ROI). (c) Visibility simulation of the radiation pattern of a portion of nanofiber scattering its guided light. We plot the visibility as a function of the nanofiber diameter, expressed in unit of λ. We consider different linear scatterer densities expressed in terms of average number of scatterers per slice of nanofiber with a thickness equal to the optical resolution. We consider scatterers randomly distributed: first, in the bulk (solid line) and second, on the surface (dashed line). We also plot measured visibilities observed in our lab (LKB) and in the literature (Vetsch, [11]).

Optics EXPRESS

resolution increases also the visibility. This is due to destructive interference in the far-field and in the direction of the dipoles as explained in the appendix A.

The measured visibilities are compatible with our simulations and support our model of light scattering by a nanofiber. This study enables to link the far-field radiation pattern to hypothesis on the microscopic properties of nanofibers, such as the distribution of the scatterer in the bulk of the nanofiber.

5. Berek compensation: iterative procedure

As reported previously, the nanofiber is expected to alter the radiation of the embedded scatterers. Now, the Berek procedure described earlier relies on Eq. (6) that gives the Stokes parameters S^1_{out} and S^2_{out}, which itself derives from the dipole-like radiation of the nanofiber. Therefore, the Berek procedure is not accurate and needs to be adapted. In the following, we present the experimental compensation procedure we applied to the 300 nm nanofiber.

We prepare linear polarization with angle φ at the input of the optical system and record the signals $I_1(\varphi)$ and $I_2(\varphi)$ of the cameras. This is performed by a motorized rotation of a half-wave plate at the input of the system as presented in Fig. 2. Measured signals $I_1(\varphi)$ and $I_2(\varphi)$ as a function of the input polarization angle φ are presented in Fig. 4. The measured signals present oscillations with a period of 180° from which we can compute the visibility:

$$V_{1,2} = \frac{I_{1,2}^{max} - I_{1,2}^{min}}{I_{1,2}^{max} + I_{1,2}^{min}}, \tag{8}$$

where $I_{1,2}^{max}$ and $I_{1,2}^{min}$ are the maximum and minimum values of the signals collected on camera 1 and 2 respectively and integrated over a ROI of approximately 200 μm as shown in Fig. 3(b). This approach is valid if the polarization in the nanofiber does not change significantly over a length comparable to the width of the region of interest (a few hundreds microns). This is the case observed in our experiment and also reported in other experimental setups [12, 23].

If the Berek compensator cancels properly the birefringence of the fiber system, linear polarizations in the input are transformed in linear polarizations in the nanofiber. This situation corresponds to having maximal visibilities of the camera signals. The Berek procedure can hence be simplified by searching to maximize the visibilities of the camera signals while rotating the input polarization.

Figure 4(a) shows camera signals when the Berek compensator adjustment is not optimal. If the fiber system is not compensated, elliptical polarization is obtained in the nanofiber region and it leads to visibilities which are not maximum. Figure 4(b) corresponds to an adjustment of the Berek compensator that maximizes the visibility on camera 1 horizontally. Hence, this Berek adjustment enables to have the polarization of the fundamental mode aligned horizontally or vertically for the appropriate input linear polarization. Figures 4(c) and 4(d) represent camera signals with maximum visibilities.

Note that, if the overall optical system (Berek + fiber system) introduces a half-wave retardation, we also expect linear polarization in the nanofiber region and hence, we will also observe maximum visibilities of the camera signals.

It is then crucial to be able to discriminate between this two adjustments of the Berek. When the optical system acts as a half-wave plate, rotation of the input linear polarization leads to a reversed rotation of the linear polarization in the nanofiber. Whereas when the optical system does not introduce any birefringence, i.e. is compensated, the rotations of the output and input linear polarizations occur in the same sense.

Since the rotation direction of the input linear polarization is known (we set it to be clockwise), it is sufficient to observe the rotation direction of the linear polarization in the nanofiber to be able to discriminate between the case of half-wave retardation and zero birefringence. The

Optics EXPRESS

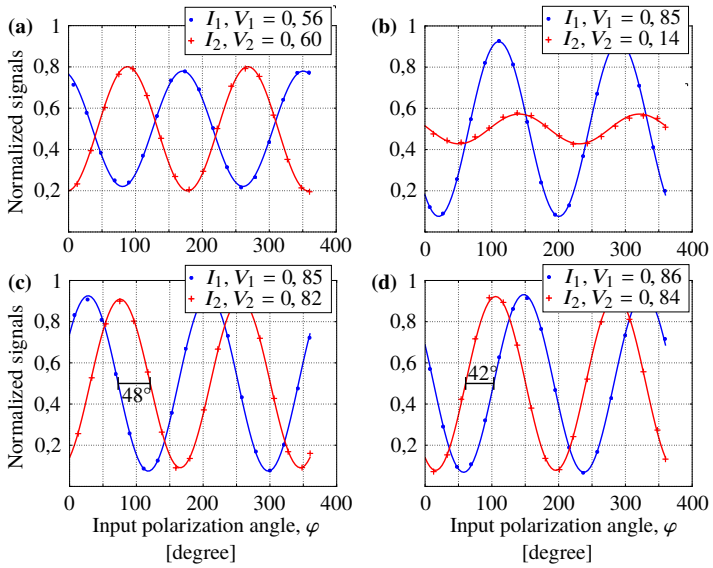

Fig. 4. Scattered signals and guided polarization. Measured signals on camera 1 and camera 2 while the input linear polarization is rotated in the clockwise direction by an angle φ. (a) Visibilities are not maximal, which corresponds to a Berek adjustments that does not compensate the fiber birefringence. (b) Visibility is maximum on camera 1, not on camera 2. This adjustment of the Berek compensator enables to align the polarization along the y (I_1 is maximal) or x (I_1 is minimal) axis. (c,d) Visibilities are maximal on both cameras simultaneously, meaning that the polarization is linear in the nanofiber region. In (c), the polarization in the nanofiber rotates in the counter-clockwise direction while the input polarization rotates in the clockwise direction, corresponding to the effect of a half-wave plate. In (d), the polarization in the nanofiber rotates in the same direction as the input polarization, corresponding to a good adjustment of the Berek compensator.

information on the rotation direction of the linear polarization in the nanofiber is contained in the relative delay between the camera signals $I_1(\varphi)$ and $I_2(\varphi)$ as we will clarify now.

When linear polarization rotates in the nanofiber, both cameras record the same signal only phase shifted according to the difference of camera angle, which is, in our case 45°. If the signal $I_1(\varphi)$ is ahead by 45° with respect to $I_2(\varphi)$, as illustrated in Fig. 4(c), it means that the polarization in the nanofiber rotates anti-clockwise. If the signal $I_2(\varphi)$ is ahead by 45° with respect to $I_1(\varphi)$, as illustrated in Fig. 4(d), the linear polarization in the nanofiber rotates clockwise.

The desired polarization mapping is hence ensured by two conditions:

- The visibilities $V_{1,2}$ are maximal.
- $I_1(\varphi)$ is delayed from $I_2(\varphi)$ by 45°.

The compensation procedure consists in fulfilling simultaneously these two conditions by playing on the two degrees of freedom of the Berek compensator. The procedure is therefore not a deductive procedure as in the ideal case but rather an iterative process of convergence toward the best compensation. Experimentally, we start by searching the Berek adjustment that ensures the correct delay between the camera signal $I_1(\varphi)$ and $I_2(\varphi)$ without considering the visibility yet. We then focus on maximizing the visibilities while keeping the proper delay.

Optics EXPRESS

6. Test of the compensation procedure

In the following, we experimentally demonstrate that the birefringence compensation procedure allows for correctly mapping arbitrary polarization states to the nanofiber. We also evaluate the typical accuracy of the mapping.

The test consists in compensating independently both sides of the nanofiber and testing the transfer of several known polarizations through the overall fiber. The setup to test the birefringence compensation is presented in Fig. 5(a). We use a first Berek compensator (Berek 1) to compensate one side of the fiber. We then use a second Berek (Berek 2) to independently compensate the birefringence of the other side of the fiber, using light propagating in the opposite direction.

The total optical system, which is the sum of two compensated systems, introduces ideally only a rotation of the input polarization. This rotation is given by the sum of the individual rotations of each fiber portion.

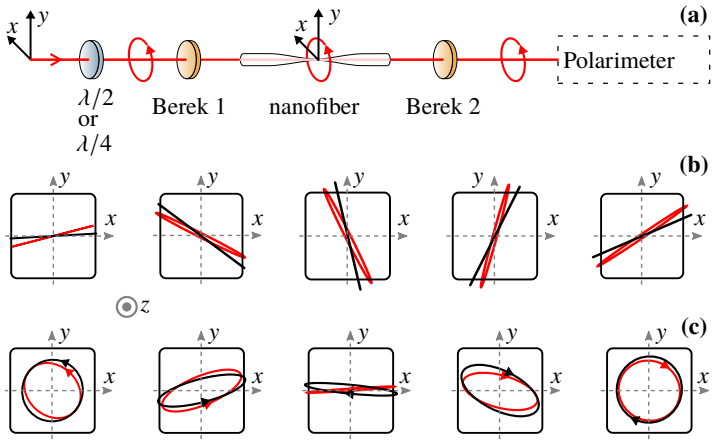

Fig. 5. Test of the birefringence compensation. (a) Experimental setup to test birefringence compensation. Each portion of the fiber setup (on the left and right side of the nanofiber) is compensated independently using Berek compensator 1 and 2 respectively. The goal is to transfer the polarization state from one side to the other with only a residual constant rotation. (b) Representation of input linear polarizations (in black) and the corresponding output polarization measured after the compensated nanofiber setup (in red). The linearity of the input polarization is maintained. A residual rotation of 11° ± 1° is observed. (c) Elliptical polarizations prepared in the entrance of the nanofiber setup and corresponding polarizations measured at the output.

To test this mapping, we prepare different known polarizations and measure the state of polarization at the output of the fiber by means of a polarimeter. We prepared a representative panel of polarizations including linearly, elliptically and circularly polarized light using half and quarter wave-plates. We show in Figs. 5(b) and 5(c) the polarization prepared at the input (black) compared to the polarization measured at the output (red). For linear input polarization, the measured output polarization is almost linearly polarized and mainly differ by a rotation of 11.1° ± 0.8°. This residual rotation is simply the sum of the individual rotations introduced by each compensated fiber portion: −64.0° for the left fiber portion, +72.9° for the right fiber portion, resulting in an expected overall rotation of 8.9°, close to the observed value. Elliptical and circular polarizations are also well mapped as can be seen in Fig. 5(c) where the rotation is also noticeable.

The accuracy of the mapping can be quantified in terms of normalized Stokes parameters. Compared to the known input normalized Stokes parameters (and correcting for the residual

Optics EXPRESS

rotation), the output Stokes parameters have a standard deviation of 0.09 corresponding to an accuracy of 95% for the polarization mapping. Note that this accuracy is given for two compensated systems in series so that the mapping for a single one is expected to be better.

7. Conclusion

We demonstrated a new scheme for fiber birefringence compensation in order to achieve full control of the polarization in an optical tapered nanofiber. The compensation procedure relies on analysing the light scattered by a nanofiber using two imaging systems with 45°-difference camera angle.

We carefully studied the case of light scattering by defects in a nanofiber. Simulations based on Mie theory indicate that the nanofiber significantly alters the radiation pattern of dipole scatterers embedded in its bulk. This effect enables to explain the reduced visibility observed for the radiation pattern of a nanofiber scattering its guided light. Our simulations and observations corroborate the model of point-like scatterer distributed in the nanofiber. More generally, we show how the far-field radiation properties give information on the microscopic distribution of scatterer in the nanofiber.

Finally, we demonstrated that the compensation procedure enables to transfer polarization state (represented by normalized Stokes parameters) to the nanofiber with an accuracy better than 95%. This work allows for a better (complete) control of nanofiber polarization and opens the way for exotic dipole trapping geometries [13] or nanofiber polarization states reading [15].

A. Appendix: effect of interference on radiation pattern visibility

In the Fig. 3(c) of the main text, we showed that an increasing number of scatterer per unit of optical resolution causes the visibility to increase. In this section, we want to explain why, based on a detailed description of the spatial dependence of radiation diagrams.

Let us consider the diffraction of a plane wave by a nanofiber, the axis of which is supposed to be along z. More specifically, we assume an incident field propagating in the x-direction and polarized linearly along the y-direction. We show in Fig. 6(a) the intensity distribution obtained in the vicinity of the nanofiber for a radiation wavelength of 638 nm, a nanofiber diameter of 300 nm and indices of refraction of 1.46 and 1.00 for the silica and air respectively.

The strong variation of index of refraction at the nanofiber surface causes the paraxial approximation to break and leads to the emergence of a field component along the direction of propagation. This non-transverse component of the electric field, E_x, is shown in Fig. 6(b).

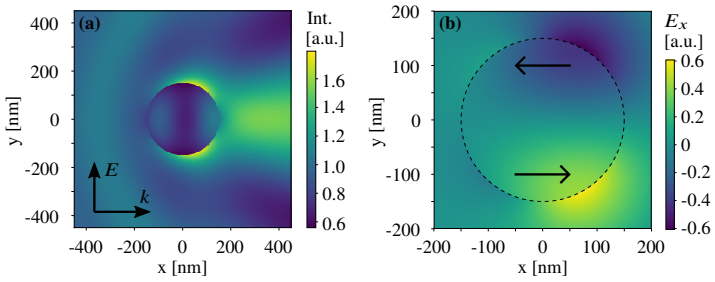

Fig. 6. Near field diffraction of a plane wave by a nanofiber. (a) Intensity distribution for an incident field polarized along y. (b) Plot of the non-transverse electric field component E_x responsible for the radiation of light along the dipole direction when it is located in the nanofiber. The black arrows indicate the direction of the field component illustrating the phase opposition between the lower and upper part of the nanofiber.

The mode of propagation considered here is therefore transverse in the far field of the nanofiber

Optics EXPRESS

(it is a plane wave) but has a non-transverse component in the vicinity of the nanofiber. A linear dipole located in the nanofiber can hence radiate light along its axis direction. As can be seen in Fig. 6(b), the amplitude of the non-transverse electric field component changes sign above and below the xz-plane. This can be understood as a consequence of spin-momentum locking in transversely decaying electric fields [26].

Consider now two dipoles contained in the xy-plane with same orientation (for example horizontal) and symmetrically located with respect to the x-axis. Taken individually, they would each radiate the same amount of light in the x-direction. But if we consider the coherent radiation of this two dipoles that oscillate in phase, they will interfere destructively in the far field x-direction. That is, they are not radiating anymore along their dipole axes as they would individually. The visibility of two symmetrical dipoles in the nanofiber is therefore 1. The visibility of the coherent radiation pattern of a large number of dipoles with same orientation tends to approach unity because each dipole has probably a symmetrical replica to interfere destructively with.

Funding

Ville de Paris (Emergence); PSL Research University (Cosine).

Acknowledgments

The authors thank Clément Sayrin, Baptiste Gouraud, Guillaume Blanquer, Elisabeth Giacobino and Jeremy Raskop for helpful discussions.

References

1. P. Solano, J. A. Grover, J. E. Hoffman, S. Ravets, F. K. Fatemi, L. A. Orozco, and S. L. Rolston, "Optical nanofibers: A new platform for quantum optics," in *Advances In Atomic, Molecular, and Optical Physics,* vol. 66 E. Arimondo, C. C. Lin, and S. F. Yelin, eds. (Academic, 2017), pp. 439–505.
2. K. P. Nayak, M. Sadgrove, R. Yalla, F. L. Kien, and K. Hakuta, "Nanofiber quantum photonics," J. Opt. **20**, 073001 (2018).
3. J. Petersen, J. Volz, and A. Rauschenbeutel, "Chiral nanophotonic waveguide interface based on spin-orbit interaction of light," Science **346**, 67–71 (2014).
4. C. Sayrin, C. Junge, R. Mitsch, B. Albrecht, D. O'Shea, P. Schneeweiss, J. Volz, and A. Rauschenbeutel, "Nanophotonic optical isolator controlled by the internal state of cold atoms," Phys. Rev. X **5**, 041036 (2015).
5. J. Volz, M. Scheucher, C. Junge, and A. Rauschenbeutel, "Nonlinear π phase shift for single fibre-guided photons interacting with a single resonator-enhanced atom," Nat. Photonics **8**, 965 (2014).
6. P. Lodahl, S. Mahmoodian, S. Stobbe, A. Rauschenbeutel, P. Schneeweiss, J. Volz, H. Pichler, and P. Zoller, "Chiral quantum optics," Nature **541**, 473–480 (2017).
7. F. Le Kien, V. I. Balykin, and K. Hakuta, "Atom trap and waveguide using a two-color evanescent light field around a subwavelength-diameter optical fiber," Phys. Rev. A **70**, 063403 (2004).
8. E. Vetsch, D. Reitz, G. Sagué, R. Schmidt, S. T. Dawkins, and A. Rauschenbeutel, "Optical interface created by laser-cooled atoms trapped in the evanescent field surrounding an optical nanofiber," Phys. Rev. Lett. **104**, 203603 (2010).
9. J. E. Hoffman, S. Ravets, J. A. Grover, P. Solano, P. R. Kordell, J. D. Wong-Campos, L. A. Orozco, and S. L. Rolston, "Ultrahigh transmission optical nanofibers," AIP Adv. **4**, 067124 (2014).
10. T. Woliński, "Polarization in optical fibers," Acta Phys. Polonica A **95**, 749–760 (1999).
11. E. Vetsch, S. T. Dawkins, R. Mitsch, D. Reitz, P. Schneeweiss, and A. Rauschenbeutel, "Nanofiber-based optical trapping of cold neutral atoms," IEEE J. Sel. Top. Quantum Electron. **18**, 1763–1770 (2012).
12. A. Goban, K. S. Choi, D. J. Alton, D. Ding, C. Lacroûte, M. Pototschnig, T. Thiele, N. P. Stern, and H. J. Kimble, "Demonstration of a state-insensitive, compensated nanofiber trap," Phys. Rev. Lett. **109**, 033603 (2012).
13. D. Reitz and A. Rauschenbeutel, "Nanofiber-based double-helix dipole trap for cold neutral atoms," Opt. Commun. **285**, 4705–4708 (2012).
14. C. Phelan, T. Hennessy, and T. Busch, "Shaping the evanescent field of optical nanofibers for cold atom trapping," Opt. Express **21**, 27093–27101 (2013).
15. M. Joos, C. Ding, V. Loo, G. Blanquer, E. Giacobino, A. Bramati, V. Krachmalnicoff, and Q. Glorieux, "Polarization control of linear dipole radiation using an optical nanofiber," Phys. Rev. Appl. **9**, 064035 (2018).
16. T. Nieddu, V. Gokhroo, and S. N. Chormaic, "Optical nanofibres and neutral atoms," J. Opt. **18**, 053001 (2016).
17. M. Sadgrove, S. Wimberger, and S. N. Chormaic, "Quantum coherent tractor beam effect for atoms trapped near a nanowaveguide," Sci. Rep. **6**, 28905 (2016).

Optics EXPRESS

18. F. L. Kien, J. Liang, K. Hakuta, and V. Balykin, "Field intensity distributions and polarization orientations in a vacuum-clad subwavelength-diameter optical fiber," Opt. Commun. **242**, 445–455 (2004).
19. R. Ulrich, S. C. Rashleigh, and W. Eickhoff, "Bending-induced birefringence in single-mode fibers," Opt. Lett. **5**, 273–275 (1980).
20. J. N. Ross, "The rotation of the polarization in low birefringence monomode optical fibres due to geometric effects," Opt. Quant. Electron. **16**, 455–461 (1984).
21. R. C. Jones, "A new calculus for the treatment of optical systems i. description and discussion of the calculus," J. Opt. Soc. Am. **31**, 488–493 (1941).
22. H. Hurwitz and R. C. Jones, "A new calculus for the treatment of optical systems ii. proof of three general equivalence theorems," J. Opt. Soc. Am. **31**, 493–499 (1941).
23. F. Lei, G. Tkachenko, J. M. Ward, and S. N. Chormaic, "Complete polarization control for a nanofiber waveguide using directional coupling," arXiv preprint arXiv:1904.05513 (2019).
24. P. W. Barber and S. C. Hill, *Light scattering by particles: computational methods*, vol. 2 (World Scientific, 1990).
25. V. Loo, G. Blanquer, M. Joos, Q. Glorieux, Y. D. Wilde, and V. Krachmalnicoff, "Imaging light scattered by a subwavelength nanofiber, from near field to far field," Opt. Express **27**, 350–357 (2019).
26. T. V. Mechelen and Z. Jacob, "Universal spin-momentum locking of evanescent waves," Optica **3**, 118–126 (2016).